Analyst

PAPER

View Article Online
View Journal | View Issue

Cite this: *Analyst*, 2023, **148**, 6050

Monitoring of *n*-hexane degradation in a plasma reactor by chemical ionization mass spectrometry†

Perla Trad, *[a,b] Nicole Blin-Simiand,[a] Pascal Jeanney,[a] Stéphane Pasquiers,[a] Joel Lemaire,[c] Essyllt Louarn,[c] Hélène Mestdagh[c] and Michel Heninger[c]

Received 21st September 2023,
Accepted 21st October 2023

DOI: 10.1039/d3an01617j

rsc.li/analyst

n-Hexane (C_6H_{14}) removal and conversion are investigated in a filamentary plasma generated by a pulsed high-voltage Dielectric Barrier Discharge (DBD) at atmospheric pressure and room temperature in a dry N_2/O_2 (20%) mixture with C_6H_{14}. The degradation of *n*-hexane and the by-product formation are analyzed in real-time using a high-resolution Fourier Transform Ion Cyclotron Resonance (FT-ICR) mass spectrometer coupled with Chemical Ionization (CI). As alkanes are reacting slowly with H_3O^+ ions, two precursor ions were used: O_2^+ to follow the *n*-hexane mixing ratios and H_3O^+ to follow the mixing ratios of organic by-products. As the CI-FTICR technique can work at high mixing ratios, studies were made between 5 and 200 ppm of *n*-hexane. Absorption spectroscopy is also used to follow ozone and carbon dioxide molecules. We show that the DBD efficiency increases for lower *n*-hexane mixing ratios and a large number of by-products are identified, with the major compounds being: formaldehyde, acetaldehyde, propanal, carbon dioxide, and carbon monoxide along with nitrate compounds. Based on the nature of the by-products characterized, a mechanism accounting for their formation is proposed.

1 Introduction

Volatile organic compounds (VOCs) group together a multitude of substances that can be of natural or anthropogenic origin. They are used in industrial processes, including around twenty activity sectors. They have proven toxicity for humans, thus justifying a rigorous classification. An overview of occupational exposures to VOCs in France was published in 2011 [1] and is regularly updated.[2] This summary work consists in identifying the VOCs most frequently measured between 2003 and 2010 that are subject to an occupational exposure limit value (VLEP). Among these substances, there are nine proven or suspected CMR (Carcinogenic, Mutagenic, and Reprotoxic) agents according to the European classification and the International Center for Cancer Research (IARC). The agents listed are toluene, styrene, formaldehyde, ethylbenzene, dichloromethane, *n*-hexane, tetrachloroethylene, trichloroethylene, and benzene.

Given the high volatility of most VOCs, workstations using VOCs are often sources of operator exposure. This can lead, if necessary, to the implementation of solutions that limit the risk of exposure or even eliminate it. While activated carbon adsorption systems are still prevalent methods to trap VOCs, air purification devices using advanced oxidation techniques have existed for several years in different sectors of activity.

Non-thermal plasmas are used in such oxidation techniques.[3,4] A non-thermal plasma is not in thermodynamic equilibrium since the electron temperature is much higher than the temperature of heavier species, which may be close to room temperature. High-velocity electrons thus react on stable molecules in the gas. This entails the formation of reactive species like atomic oxygen O, hydroxyl radical OH, and metastable nitrogen species N_2*. In the presence of organic molecules in the gaseous mixture, removal processes initiated by these reactive species lead to the total or partial oxidation of the polluting compounds. Since the beginning of the 1990s, a great amount of work has been performed on the conversion of VOCs by non-thermal plasmas produced in mixtures of atmospheric gases $N_2/O_2/H_2O$.

Several studies have been published concerning VOCs removal by these plasmas or their coupling with different types of catalysts, they concern various types of molecules: hydrocarbons,[5,6] carbonyl compounds,[7,8] and alcohols.[9] Multiple ways of producing plasma with pulsed electrical discharge have been reported,[10–19] such as Dielectric Barrier Discharge (DBD) and packed-bed plasma reactors.

The pollutant investigated in this study, *n*-hexane, a highly toxic VOC, is found in different types of industries where it is

[a]*Université Paris-Saclay, CNRS, Laboratoire de Physique des Gaz et des Plasmas, 91405 Orsay, France. E-mail: perla.trad@universite-paris-saclay.fr*
[b]*Institut National de Recherche et de Sécurité, Rue du Morvan, CS60027, 54519 Vandœuvre Cedex, France*
[c]*Université Paris-Saclay, CNRS, Institut de Chimie Physique, 91405 Orsay, France*
† Electronic supplementary information (ESI) available. See DOI: https://doi.org/10.1039/d3an01617j

heavily used as an industrial solvent. Due to *n*-hexane's long carbon chain, its treatment generates numerous by-products from different chemical families, whose formation mechanism is not yet well established.

Studies concerning products issued from controlled oxidation of *n*-hexane were published for temperatures between 450–1000 K at 1 atm.[20,21] Experiments in a jet-stirred reactor in the temperature range of 530–1160 K at 10 atm allow for the identification of species and measure their mixing ratio as functions of temperature. The results were used to validate a chemical kinetic model for the *n*-hexane oxidation mechanism.[22]

For the studies concerning *n*-hexane degradation with different plasma reactors,[23–27] none of them uses PTR-MS instruments (Proton Transfer Reaction Mass Spectrometry) for gas analysis. PTR-MS use proton transfer from H_3O^+ ions to ionize specifically the VOCs present which are then detected by mass spectrometry. It is implemented with different kinds of mass spectrometers such as quadrupole,[28] time of flight[29] or FTICR.[30] It is a very sensitive technique for the real time analysis of VOCs and has applications in many areas: atmospheric research, food analysis, heath monitoring.[31,32]

Only in a few cases PTR-MS instruments have been applied to the determination of plasma degradation products: results are available for acetone,[8,33] toluene,[3] 2-heptanone,[34] ethyl acetate.[35] The precursor ions used in all these studies are H_3O^+ ions, since they are quite efficient in detecting the target VOCs and most of their degradation products, and only in the case of acetone, O_2^+ ions were also used to detect alkane degradation products. In the case of *n*-hexane a difficulty is that H_3O^+ ions do not react or react very slowly with *n*-hexane. In general the study of alkanes by mass spectrometry coupled to chemical ionization in PTR-MS instruments is difficult since alkanes do not give stable protonation products with the H_3O^+ ions, and the rate coefficients are not known.

To solve this problem, we have used two different ionic precursors in the CI-FTICR analyzer: O_2^+ for the detection of *n*-hexane (and some of the by-products) and H_3O^+ for the detection of most degradation products. High mixing ratio such as the one used for *n*-hexane are often a problem PTR-MS instruments: those based on chemical ionization in a drift tube operated at pressures close to 1 mbar are very sensitive and able to detect VOCs with mixing ratio <1 ppt but in order to deal with high mixing ratio a dilution in air in necessary. This is not the case with CI-FTICR instrument in which the reaction time can be adjusted resulting in a range of accessible mixing ratio from ~10 ppb up to a few %.

Therefore studying *n*-hexane plasma degradation by CI-FTICR is interesting for trace analysis in a complex mixture, allowing (i) to validate the consistency of the different analytical methods used, (ii) to understand the physicochemical processes involved.

In this study, we present the removal of *n*-hexane by a non-thermal plasma reactor, in order to evaluate its efficiency, while analyzing the treated effluents to quantify the by-products that can be issued from the degradation of the molecule.

2 Materials and methods

2.1 Plasma discharge reactor

A scheme of the experimental set-up, similar to that already described for the treatment of toluene,[3] is given in Fig. 1. The plasma reactor consists of an alumina tube (internal diameter 10 mm, thickness 2.5 mm, permittivity ε_r = 9.05) functioning as a dielectric barrier. On its exterior is an electrically grounded copper tape (5 cm length). At the center of the tube, a tungsten rod, with a diameter of 1 mm, is connected to a high-voltage power supply. These elements make it possible to generate a DBD in a cylindrical coaxial geometry with a reactor volume of 3.9 cm^3. The plasma is created at atmospheric pressure and at room temperature in dry synthetic air (20% oxygen). The *n*-hexane-containing gas mixture was prepared and introduced into the reactor using a GasMix™ Zephyr (AlyTech, Juvisy, France) gas diluter from a calibrated air/*n*-hexane standard mixture (500 ppm, Crystal mixture Air Liquide) and dry synthetic air, for a total volumetric flow rate of 0.5 L min^{-1} NTP. The resulting mixing ratio of *n*-hexane in the gas before treatment varies from 5 ppm to 200 ppm.

2.2 Electrical characterization

For most of the results discussed in this paper, the DBD was driven by HV pulses at a repetition frequency, f = 500 Hz. At this repetition frequency and flow rate, the gas will be treated with about 234 HV-pulses before exiting the reactor. The applied voltage (peak value measured on a purely capacitive load, without plasma) was chosen in the range between 17 kV and 24 kV.

The electrical energy deposited in the plasma during each HV-pulse, E_{pulse}, was determined through measurements of the voltage, $V(t)$, and current, $I(t)$, and integration of the instantaneous electrical power over the duration of one pulse:

$$E_{pulse} = \int V(t)I(t)\mathrm{d}t \quad (1)$$

This method allowed real-time energy monitoring; for each experiment, E_{pulse} was systematically followed throughout the discharge operation. E_{pm}, the mean energy values were calculated over several thousand pulses. Current and voltage waveforms were measured by means of electrical probes (Lecroy PPE, TM Research Products SBNC-5-5) connected to a fast digital oscilloscope (Lecroy 204 MXi-A, 2.0 GHz, 10 GS s^{-1}, New York US).

The energy deposited into the plasma per unit of volume, *i.e.* the specific energy, SED is defined by the following:

$$\mathrm{SED} = \frac{E_{pulse} \cdot f}{Q} \quad (2)$$

where Q is the total gas flow rate and f is the HV-pulse repetition frequency.

Plotted in Fig. 2 are examples of current and voltage temporal evolutions measured for the gas mixture containing

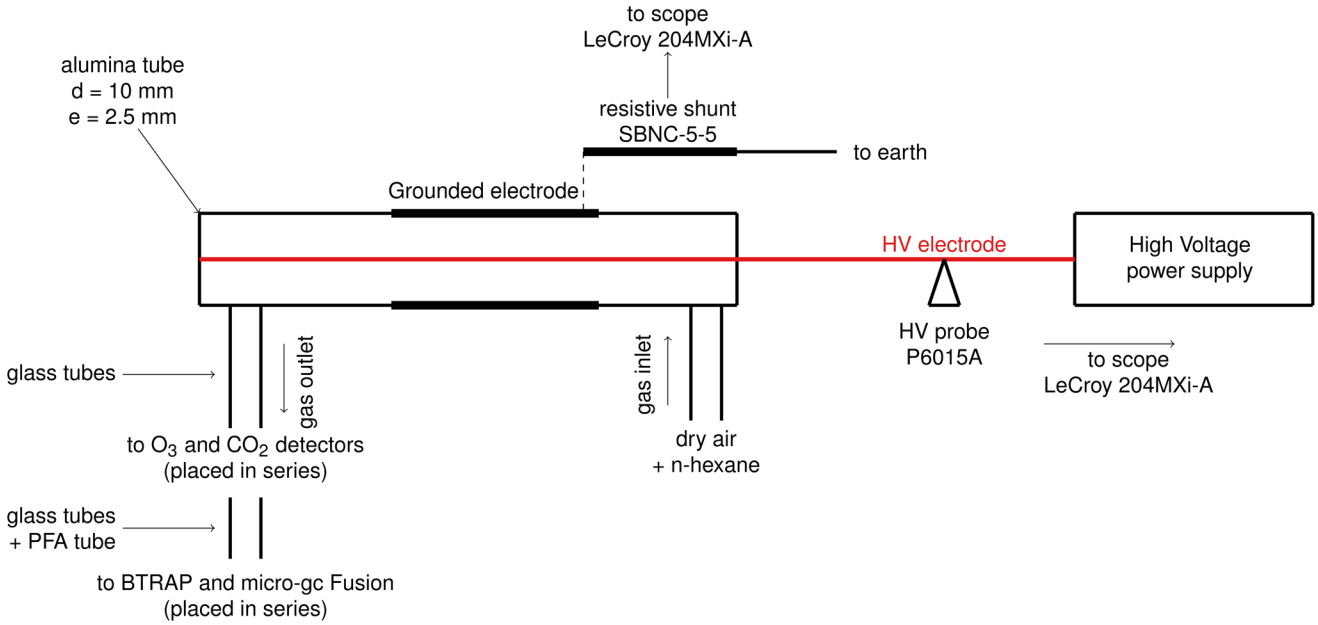

Fig. 1 Schematic drawing of the experimental set-up.

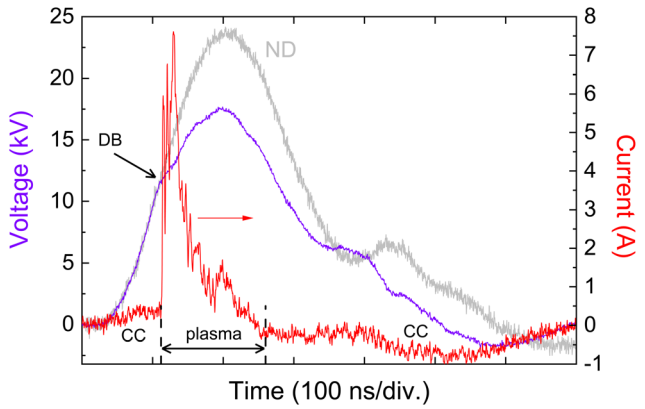

Fig. 2 Typical temporal evolutions of current and voltage. HV-pulse repetition frequency: 500 Hz, applied voltage: 23.6 kV (ND: no discharge, voltage plot in grey line), gas flow rate: 0.5 L mn^{-1} NTP, *n*-hexane mixing ratio: 100 ppm. DB: discharge breakdown, CC: capacitive current.

100 ppm of *n*-hexane, and other parameters indicated in the figure caption.

2.3. Analytical methods

2.3.1 Analytical techniques. After treatment through the DBD device, the treated effluents were analyzed at the exit of the reactor by different methods: (i) ozone measurement using a UV analyzer (Ozone analyzer BMT 964, BMT MESSTECHNIK GMBH, Hamburger, Germany) at 254 nm, (ii) CO_2 and H_2O measurements with a Li-840 gas analyzer by absorption in the infra-red (carbon dioxide: 4.26 μm, water = 2.59 μm, LICOR, Lincoln, US), (iii) VOC and *n*-hexane measurements using CI-FTICR (Chemical Ionization Fourier Transform Ion Cyclotron Resonance) mass spectrometer BTrap (AlyXan, Juvisy, France), (iv) *n*-hexane, CO and H_2 measurements using a micro gas chromatograph with thermal conductivity detection equipped with a molecular sieve column and a PDMS column (GC-TCD; Micro GC Fusion, Chemlys, Vénissieux, France). The *n*-hexane is measured on the PDMS column (T = 70 °C, P = 21.5 psi, l = 10 m, d_i = 0.15 mm), CO and H_2 are measured on the molecular sieve column (T = 70 °C, P = 30 psi, l = 10 m, d_i = 0.25 mm).

2.3.2 CI-FTICR mass spectrometer. Mass spectrometry coupled with chemical ionization (CI) is widely used for online measurement of VOCs. The instrument used for this study is a high-resolution Fourier Transform Ion Cyclotron Resonance (FT-ICR) mass spectrometer commercialized by AlyXan company. This instrument described elsewhere[30,36] is based on a permanent magnet generating a magnetic field of 1.5 Tesla. In this instrument, the ICR cell placed in the magnet is used successively as an ion source, reaction chamber, and analyzer. The intensity of the peaks on the mass spectrum, obtained after Fourier Transformation of the image current induced by the rotating ions is not mass-dependent, therefore no correction of intensities is required.[36] It is able to detect VOCs in trace amounts from tens of ppb to % with a detection every 3 s (ESI Fig. 2†).

It allows absolute quantification of the compounds identified based on the relative intensities of the ions and the CI reaction rate coefficient. The high mass resolution allows good identification of molecular formulas, making it possible to separate quasi-isobaric compounds and follow their mixing ratio during the experiment.

Chemical ionization is based on the use of a selective ion-molecule reaction to ionize and detect the compounds of interest. Different precursor ions may be used in positive mode

such as H_3O^+,[37] CF_3^+,[38] $C_6H_4F_2$–H^+[39] or negative mode, such as HO^-, O^-.[40] For this study two precursor ions were used, O_2^+ and H_3O^+. With H_3O^+ precursor the main CI reaction is protonation of the analyte A leading to AH^+ ion, provided its proton affinity PA(A) is higher than PA(H_2O) = 691 kJ mol^{-1}. Quite differently, O_2^+ reacts by initial charge transfer giving A^+, generally followed by fragmentation. The energy of the trapped ions remains very low, it is acquired solely from the exothermicity of the CI reaction, which may lead to the fragmentation of the ions produced. This charge transfer is fast with most VOCs.

Thus, H_3O^+ is well suited for the detection of *n*-hexane oxidation products in the discharge effluents since these products are oxygenated or unsaturated molecules with relatively high PAs. Towards alkanes such as *n*-hexane, H_3O^+ has a low reactivity since PA(*n*-hexane) = 676 kJ mol^{-1} < PA(H_2O);[41] H_3O^+ is not appropriate for *n*-hexane quantification.

Therefore, the O_2^+ ion was used to measure the degradation rates of *n*-hexane as a function of the deposited energy and initial *n*-hexane mixing ratio, while H_3O^+ allowed analysis of its partial oxidation products in the plasma. The reaction of O_2^+ ion with *n*-hexane is known to be fast with many fragmentation pathways. A slow reaction between the H_3O^+ ion and *n*-hexane was observed. Accordingly, we have started this study by re-measuring the rate coefficients and branching ratios of the reactions of O_2^+ and H_3O^+ with *n*-hexane in our experimental conditions.

In the case of a complex mixture such as the DBD effluents under study, interpretation of the O_2^+ results is made difficult by the large numbers of fragmentation pathways. Moreover, the rate coefficients and branching ratios of the reactions of O_2^+ are not well known for all VOCs of interest. For these different reasons, the O_2^+ ion will be mainly used to quantify *n*-hexane and products that cannot be detected with the H_3O^+ ion.

In consequence, *n*-hexane mixing ratio is measured by CI-FTICR-MS using O_2^+ as precursor ion for the mixing ratios in the range of (5 ppm–200 ppm) and by Micro GC for mixing ratios in the range of (50 ppm–150 ppm).

VOCs by-product formation is followed by CI-FTICR-MS using H_3O^+ as precursor ion. The mixing ratios are calculated using the experimental rate coefficients, when available, or using the capture rate coefficient calculated from Su and Chesnavich formula.[42] NO_x and C_2H_4 are monitored using O_2^+ precursor ion.

If rate coefficients are known, absolute quantification of detected molecules is possible.

The mixing ratio of the molecules detected with the H_3O^+ precursor in the mass spectrometer[30] when no fragmentation occurs on the AH^+ ion, is calculated with the following equation:

$$[\mathrm{M}] = \frac{\ln\left(\frac{\mathrm{Sum}}{I_{\mathrm{H_3O^+}}}\right) \times I_{\mathrm{AH^+}} \times 10^6}{(\mathrm{Sum} - I_{\mathrm{H_3O^+}}) \times k \times P \times t \times 3.21} \quad (3)$$

where I_{AH^+} and $I_{H_3O^+}$ are the signal intensities of the AH^+ and H_3O^+ ions respectively, k (10^{-9} molecule^{-1} cm^3 s^{-1}) is the reaction coefficient between the molecule M and the H_3O^+ ion, and $P \times t$ is equal to the integrated value of the pressure observed during the experiment between gas sample introduction and detection. The Sum refers to the sum of signal intensities of all the detected ions.

2.3.3 Operating sequence. In most of the experiments, we worked at a given SED and an applied voltage of 23.6 kV, while keeping the repetition frequency at 500 Hz and the gas flow rate at 0.5 L min^{-1}, and changed the mixing ratio of *n*-hexane introduced into the reactor. The discharge operates continuously throughout the experiment.

Firstly, the discharge is started in synthetic air at a given SED. At this step, the chemical noise is measured, *i.e.* the by-products that could be produced by residual pollution in the tubes, this corresponds to measurements with 0 ppm of *n*-hexane. The chemical noise value is then subtracted from any result obtained with *n*-hexane to eliminate the effect of pollution in our system.

Secondly, *n*-hexane is introduced into the discharge at a certain mixing ratio, and the generated by-products are measured.

These two steps are repeated for several mixing ratios of *n*-hexane while keeping the discharge running and all operating conditions constant.

Lastly, the interior walls of the tubes are cleaned, by running a discharge in air.

3 Results and discussion

3.1 Rate coefficient measurements

To quantify the *n*-hexane mixing ratio, the rate coefficient of the reaction of O_2^+ with *n*-hexane was measured in our experimental conditions. The reaction of H_3O^+ with *n*-hexane, which is known to be very slow, was also studied. The rate coefficients were measured in the absence of discharge and under chemical ionization conditions using the gas cylinder of 500 ppm *n*-hexane in an air matrix and diluting it with synthetic air in the 5–200 ppm range.

3.1.1 Reactivity of O_2^+ with *n*-hexane. The reaction of the O_2^+ ion with *n*-hexane C_6H_{14} (4) is a charge transfer reaction that is exothermic by about 193 kJ mol^{-1}.[43]

The main reaction channels are the formation of the fragments ions $C_4H_9^+$ (6) and $C_4H_8^+$ (7), then charge transfer to $C_6H_{14}^+$ (4). These results are similar to those reported by Francis *et al.*[44] given in parentheses for a CI pressure of 0.25 Torr. Since the CI reaction occurs at lower pressure (*ca.* 10^{-5} Torr) in our instrument, we expect to get a larger fragmentation extent. The agreement with Francis's results is thus quite good. The somewhat lower fragmentation in the flow tube experiment could be explained by some collisional relaxation at the much higher pressure (0.25 Torr) used.

$$O_2^+ + C_6H_{14} \rightarrow C_6H_{14}^+ + O_2 \quad 11\% \quad (20\%) \quad (4)$$

$$\rightarrow C_5H_{11}^+ + O_2 + CH_3 \quad 3\% \quad (5\%) \quad (5)$$

$$\rightarrow C_4H_9^+ + O_2 + C_2H_5 \quad 37\% \quad (35\%) \tag{6}$$

$$\rightarrow C_4H_8^+ + O_2 + C_2H_6 \quad 32\% \quad (25\%) \tag{7}$$

$$\rightarrow C_3H_7^+ + O_2 + C_3H_7 \quad 8\% \quad (5\%) \tag{8}$$

$$\rightarrow C_3H_6^+ + O_2 + C_3H_8 \quad 8\% \quad (10\%) \tag{9}$$

Three minor channels with less than 1% were also observed: $C_4H_7^+$, $C_6H_{13}^+$, $C_5H_1O^+$.

The total rate coefficient measured is 1.9×10^{-9} molecule^{-1} cm^3 s^{-1} in good agreement with previous experimental values: 1.7–1.9 $\times 10^{-9}$ molecule^{-1} cm^3 s^{-1} (ref. 44) or with the capture rate coefficient, 1.8×10^{-9} molecule^{-1} cm^3 s^{-1}.[42]

3.1.2 Reactivity of H_3O^+ with *n*-hexane. Under our experimental conditions, four products were detected, and a total reaction rate coefficient of 1.9×10^{-11} molecule^{-1}cm^3 s^{-1} was measured (Fig. 3):

We observe a linear evolution of the products as a function of injected *n*-hexane with correlation coefficients of 0.99 for all products.

$$H_3O^+ + C_6H_{14} \rightarrow C_3H_7^+ + H_2O + C_3H_8 \quad 24\% \tag{10}$$

$$\rightarrow C_4H_9^+ + H_2O + C_2H_6 \quad 44\% \tag{11}$$

$$\rightarrow C_5H_{11}^+ + H_2O + CH_4 \quad 3\% \tag{12}$$

$$\rightarrow C_6H_{13}^+ + H_2O + H_2 \quad 29\% \tag{13}$$

Arnold *et al.*[45] studied the reactivity of H_3O^+ ion with C_2–C_{12} alkanes. For *n*-hexane they measured an overall rate coefficient at 300 K of 3×10^{-11} molecule^{-1} cm^3 s^{-1} with two main products: $C_6H_{14}H_3O^+$ (association product 63%) and $C_6H_{13}^+$ ion (20%) and the formation of minor products $C_4H_9^+$ (4%), $C_4H_9OH_2^+$ (3%) and $C_3H_7OH_2^+$ (10%).

Proton transfer reaction of H_3O^+ ions with *n*-hexane is endothermic by 15 kJ mol^{-1} and is expected to be very slow. The pressure conditions in our experiment are also much lower than 10^{-5} Torr compared to those used in SIFT techniques (~0.45 Torr) therefore the association product cannot be observed.

The value of the rate coefficient measured here is inferior to the value measured by Arnold as the association reaction is not possible.

3.2 *n*-Hexane degradation

The mixing ratios of *n*-hexane are calculated from the measurement of the $C_6H_{14}^+$ ion intensities using the rate coefficient and the branching ratio measured in this study. Fig. 4 shows the evolution of the total removal efficiency, defined as the ratio of removed mixing ratio to injected mixing ratio (reactor inlet), as a function of the mixing ratio of *n*-hexane injected.

$$\text{Efficiency}\,(\%) = \frac{[C_6H_{14}]_0 - [C_6H_{14}]}{[C_6H_{14}]_0} \times 100 \tag{14}$$

The degradation is more efficient for the low injected mixing ratios. This result is in good agreement with previous studies concerning plasma treatment in air of various molecules.[46,47] The results obtained with the two techniques are in good agreement in the (50 ppm–200 ppm) range as shown in Fig. 4.

3.3 By-products

The treatment of *n*-hexane by the plasma is initiated by an oxidation reaction with atomic oxygen and hydroxyl radical, leading to radical formation on one of the carbon atoms of *n*-hexane. This radical rapidly reacts in different ways with the components of the discharge mixture. This leads to the production of several VOCs alongside CO, H_2O, CO_2, and H_2. Ozone is also generated in atmospheric plasmas; however, it is not an oxidation by-product (ESI: Fig. 4†).

3.3.1 CO_2, CO and H_2O production. The CO_2 and CO results obtained for different mixing ratios of *n*-hexane are presented in Fig. 5 and H_2O results are presented in Fig. 6. CO_2 and CO are final products of the kinetic chain, and H_2O starts to appear in the oxidation initiation reactions and is also generated from oxidation reactions along the kinetic chain. The

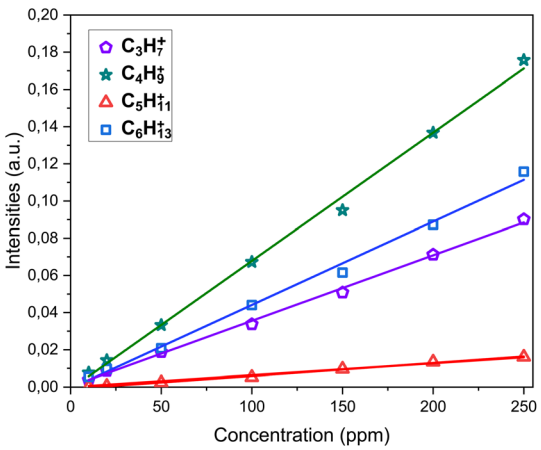

Fig. 3 Intensities of the products issued from H_3O^+ reaction with *n*-hexane as a function of *n*-hexane mixing ratio.

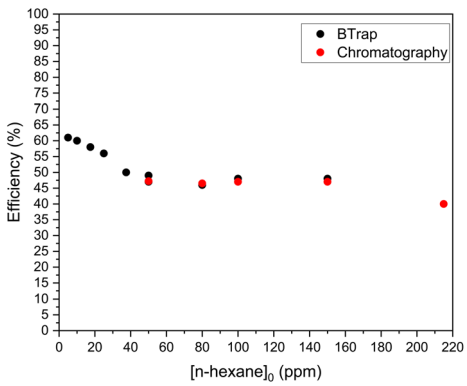

Fig. 4 Efficiency of the degradation of *n*-hexane as a function of the mixing ratio of *n*-hexane injected (SED = 265 J L^{-1}, applied voltage: 24.3 kV, HV-pulse repetition frequency: 500 Hz, gas flow rate = 0.5 L min^{-1}).

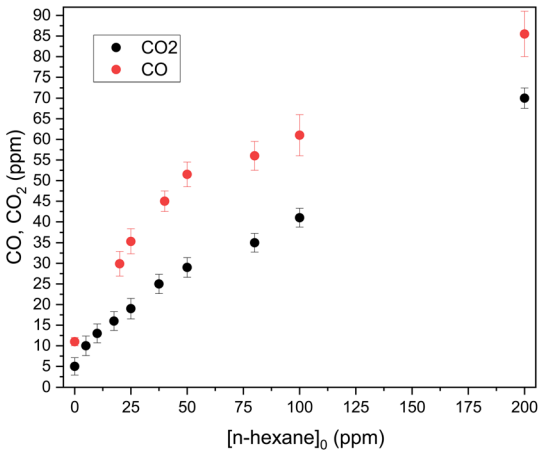

Fig. 5 Measurement of CO_2 mixing ratio (black) and CO mixing ratio (red) at the exit of the DBD for mixing ratios of *n*-hexane in air up to 200 ppm (SED: 225 J L^{-1}, applied voltage: 23.4 kV, HV-pulse repetition frequency: 500 Hz, gas flow rate: 0.5 L min^{-1}). Measurements are obtained using different detectors: CO by gas chromatography and CO_2 by IR detector.

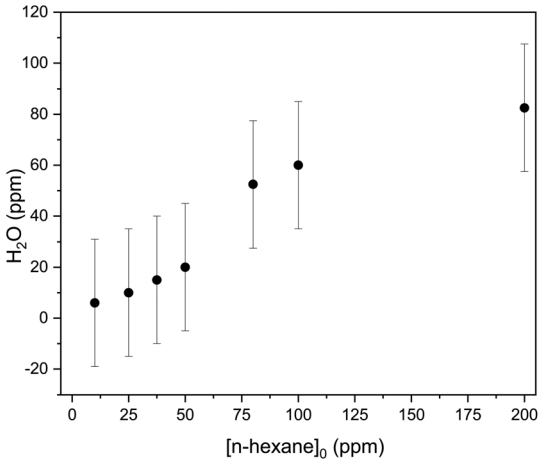

Fig. 6 Measurement of H_2O mixing ratio at the exit of the DBD for mixing ratios of *n*-hexane in air up to 200 ppm (SED: 225 J L^{-1}, applied voltage: 23.4 kV, HV-pulse repetition frequency: 500 Hz, gas flow rate: 0.5 L min^{-1}).

higher the inlet *n*-hexane mixing ratio is, the higher the by-product concentrations are. CO_2 and CO are observed even in the discharge in air without *n*-hexane, this can be explained by the treatment of deposits, CO_2 is measured at 5 ppm and CO at 11 ppm.

As shown in Fig. 6 H_2O mixing ratio steadily increases from [*n*-hexane] = 10 ppm to [*n*-hexane] = 200 ppm.

The experimental results are to be compared with the maximal possible CO_2 mixing ratio, *i.e.* the value $[CO_2]_{max}$ that would be obtained if all of the *n*-hexane consumed in the reactor was totally converted to CO_2 and H_2O. $[CO_2]_{max}$ is equal to 6 times the mixing ratio of *n*-hexane degraded in the plasma reactor. For a 50 ppm injected *n*-hexane mixing ratio, the mixing ratio of removed *n*-hexane is known from the data reported in Fig. 4 and is equal to 25 ppm. Therefore $[CO_2]_{max}$ is equal to 150 ppm. This value is higher than the CO_2 mixing ratio measured experimentally at the discharge exit, with $[CO_2]_{exp}$ = 29 ppm, as shown in Fig. 5. Taking into account the chemical noise measured in the absence of *n*-hexane, we obtain: $[CO_2]_{exp}$ = 16% $[CO_2]_{max}$. Only 16% of the carbon in the treated *n*-hexane was converted into CO_2, this indicates that the remaining carbon was converted into intermediate by-products.

3.3.2 H_2 production. H_2 is issued from dissociation reactions of *n*-hexane with nitrogen reactive species or from electron dissociation.[48] It appears on the gas chromatographer when at least 40 ppm of *n*-hexane is treated, and is observed in very small amounts (Table 1). H_2 mixing ratio steadily increases as a function [*n*-hexane]. The corresponding curve is linear, with a slope of 0.023 and a regression coefficient R^2 = 0.99 (ESI Fig. 4†).

3.3.3 By-product analysis. Fig. 7 and 8 give an example of the mass spectrum obtained when the DBD discharge is on, for a mixing ratio of 100 ppm with O_2^+ and H_3O^+ precursor ions, respectively. The absolute quantification for each product is deduced from the relative intensities of the ions, the $P \times t$ parameter measured by Btrap, and the reaction rate constant CI, according to (3).

With O_2^+ precursor ion, the main ions detected are those of the reaction of the O_2^+ ion with *n*-hexane: $C_4H_8^+$, $C_4H_9^+$, $C_6H_{14}^+$ (since this reaction is exothermic). O_2^+ is mainly used

Table 1 H_2 mixing ratio at the exit of the DBD for mixing ratios of *n*-hexane in air (SED: 225 J L^{-1}, applied voltage: 23.4 kV, HV-pulse repetition frequency: 500 Hz, gas flow rate: 0.5 L min^{-1})

[*n*-hexane]$_0$ (ppm)	40	50	80	100	200
H_2 (ppm)	0.71	1.16	1.61	1.88	4.48

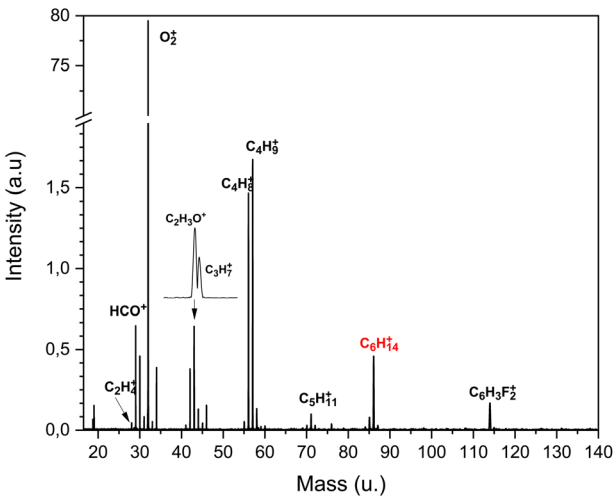

Fig. 7 Mass spectra obtained for the O_2^+ precursor ion for an *n*-hexane mixing ratio of 100 ppm, with $C_6H_4F_2^+$ being used as an internal mass calibrant (*m*/*z* 114.028).

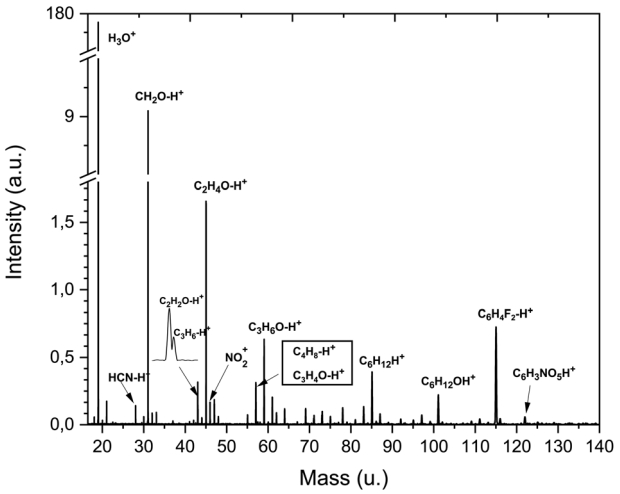

Fig. 8 Mass spectra obtained for the H_3O^+ precursor ion for an *n*-hexane mixing ratio of 100 ppm, with $C_6H_4F_2^+$ being used as an internal mass calibrant (*m*/*z* 114.028).

to measure the evolution of the *n*-hexane mixing ratio with the discharge conditions. Small organic compounds not reacting with H_3O^+ are also detected like ethylene, NO and NO_2.

As H_3O^+ precursor ion reacts very slowly with *n*-hexane, the main ions detected are the by-products of the discharge. H_2 is a by-product that is not detected on the BTrap, but is detected with gas-chromatography at very low concentrations.

3.3.4 By-products detected with H_3O^+ precursor. These by-products are listed below, classified according to their likely functional group.

• Aldehydes: The major compound detected is formaldehyde. The chemical noise for the formaldehyde is quite high, about 50 ppm, probably due to polymerization leading to solid formaldehyde polymer dust deposited in the connection tubings. Acetaldehydeis the second most abundant by-product. Propanal or acetone, that cannot be distinguished, is also detected. Hexanal and/or hexanones are detected in mixing ratios lower than 500 ppb for a mixing ratio of *n*-hexane of 50 ppm injected in the reactor.

• Small oxygenated compounds: methanol, ketene, acetic acid, hexanal, or hexanones are detected in mixing ratios lower than 500 ppb for the same injected hexane mixing ratio.

• Alkenes: propene, hexene and hexadiene C_6H_1O are detected. The corresponding detected ions (protonated alkenes) may also be due to propanol, hexanol, or hexenol *via* dehydration accompanying alcohol protonation by H_3O^+.

• Nitrite and nitrate compounds: nitrous acid, nitromethane, nitric acid, methyl nitrate, ethyl nitrate. Peroxyacetyl nitrate (PAN, $C_2H_3NO_5$ leading to *m*/*z* 122.009 ion) was also measured. In addition to these nitrogen-containing compounds, a small quantity of hydrogen cyanide is detected. The generation of HCN under our experimental conditions cannot be explained by oxidation but rather reactions between *n*-hexane and nitrogen metastable states like in the case of H_2.[48]

Fig. 9 shows the variation of the mixing ratio of the main by-products detected with H_3O^+ precursor for different *n*-hexane mixing ratios injected in the reactor. The by-products show a quite linear evolution as a function of *n*-hexane mixing ratio.

3.3.5 Combining H_3O^+ and O_2^+ precursor ions. NO^+ and NO_2^+ ions are observed with both precursors. The reactions of O_2^+ on NO and NO_2 are exothermic with rate coefficient around 8×10^{-10} cm^3 s^{-1}. H_3O^+ precursor ion does not react with NO_2 or NO. Consequently, the NO_2^+ or NO^+ ions observed with the H_3O^+ precursor ion come from fragmentations, as observed by Thomas *et al.*[33] For example, the reaction of H_3O^+ ion with N_2O_5 produces NO_2^+ ions. The mixing ratios measured for NO and NO_2 (ESI Table 1†) are global values for all the neutrals whose reactions with H_3O^+ yield NO^+ and NO_2^+ respectively.

The main by-products: formaldehyde, acetaldehyde, and propanal were also detected with the O_2^+ precursor ion, but they are more difficult to quantify because of the numerous fragmentations. More interestingly, ethylene which is not detectable by H_3O^+, was detected at low mixing ratios: 0.76 ppm for 50 ppm and 1.65 ppm for 100 ppm of *n*-hexane injected, respectively.

Since only a small proportion of carbon from consumed *n*-hexane appears as CO_2 after degradation and we have measured the mixing ratios of numerous carbon-containing by-products, it is interesting to estimate the global "elemental carbon mixing ratio" $(C)_{exp}$ in the measured VOC by-products. $(C)_{exp}$ is expressed in ppmC as:

$$\left((C)_{exp} = \sum_i (N_{ci} \times B_i)\right), \quad (15)$$

where B_i is a by-product and $[B_i]$ its measured mixing ratio, N_{ci} is the number of carbon atoms in the B_i molecule.

According to the data reported in Fig. 9, we find for a 50 ppm injected *n*-hexane mixing ratio: $(C)_{exp}$ = 43.7 ppmC. This value is about twice $(CO_2)_{exp}$, and 27.5% of $(CO_2)_{max}$.

According to gas chromatography measurements in the same experimental conditions, for a 50 ppm injected *n*-hexane mixing ratio, we find a mixing ratio of CO equal to 40 ppm.

Finally, the summed experimental mixing ratios of CO_2, CO, and carbon in VOC products account for *ca.* 108 ppmC, representing 66–67% of the degraded *n*-hexane carbon. The undetected carbon may be in the form of soot.[49]

3.3.6 Suggestions for a mechanism of formation of by-products issued from *n*-hexane conversion in air plasma. The initiation reaction is H atom abstraction from the various CH bonds by the reaction of *n*-hexane with O or OH leading to an alkyl radical C_6H_{13}.

$$C_6H_{14} + O \rightarrow C_6H_{13}^{\bullet} + OH^{\bullet}$$

$$C_6H_{14} + OH^{\bullet} \rightarrow C_6H_{13}^{\bullet} + H_2O$$

The molecule is symmetrical, three alkyl radicals are therefore possible depending on the site of H abstraction: C_1, C_2, or

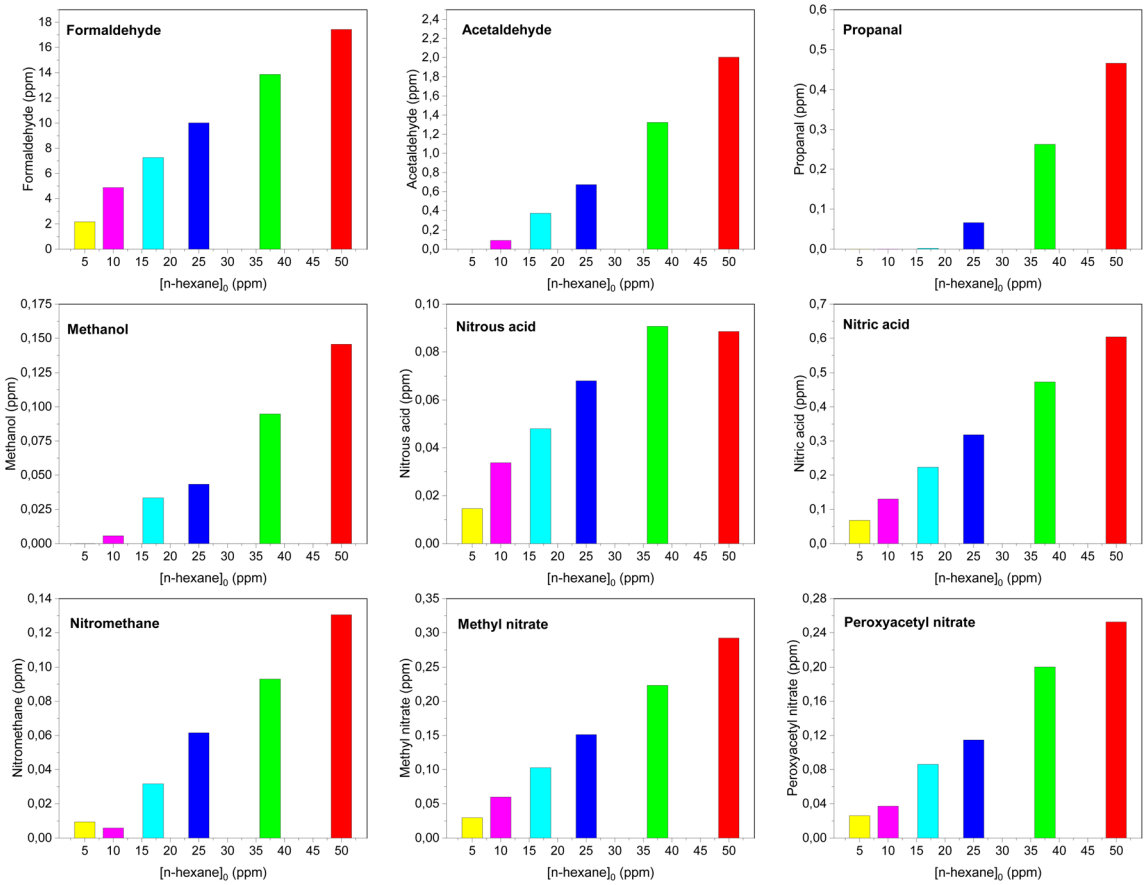

Fig. 9 Mixing ratios of the main by-products detected as a function of the mixing ratio of *n*-hexane injected.

C_3. A scheme for the first reaction steps is given in Fig. 10. Each alkyl radical issued from these initiation reactions can react in different ways: oxidation, C–C cleavage, H abstraction or NO_2 addition, NO_2 being produced in plasma of N_2/O_2 mixture.

The abstraction of a hydrogen atom in α of the different hexyl radicals may lead to the formation of different isomers: 1-, 2- and 3-hexene C_6H_{12}. Protonated hexene $C_6H_{13}^+$ ion is observed by the BTrap.

C–C cleavage leads to a shorter alkene (1-pentene, propene or 1-butene) and a shorter alkyl radical (methyl, ethyl, 1-propyl). Those alkyl radicals being very reactive, they enter into the same reaction process as that of hexyl, leading to shorter molecules.

The process that best explains the identified by-products is that of oxidation by the addition of O_2 on each hexyl radical, leading to three isomers of peroxy radicals $C_6H_{13}O_2$. These radicals lead rapidly to alkoxy radicals $C_6H_{13}O$ by reactions with NO, O or O_3.

Alkoxy radicals, RO, are reactive species, which may lead to carbonyl compounds either by H abstraction on the radical carbon atom or by C–C cleavage in β position yielding an aldehyde and a shorter radical. In this way 1-hexoxy radical leads to formaldehyde, CH_2O, and 1-pentyl radical. Two possibilities exist for 2-hexoxy radical, leading to acetaldehyde and 1-butyl radical or butanal with ethyl radical. Similarly, 3-hexoxy radical yields propanal and butanal, along with 1-propyl and1-ethyl radicals respectively. As shown in Fig. 10, the operation of this mechanism on the three hexoxy isomers allows to explain the formation of aldehydes with 1 to 6 carbon atoms, along with C_1–C_5 radicals which in turn undergo O_2 addition and so forth.

Aldehydes are actually the major by-products characterized, with formaldehyde representing *ca.* 67% of the total by-products. The presence of formaldehyde is consistent with the proposed mechanism since all the C–C cleavage chains all end with a CH_3 radical leading to CH_3O and $CH_2{=}O$.

Alkyl or alkoxy radicals can also react by addition with NO_2 to give RNO_2 and $RONO_2$ respectively. While CH_3NO_2 is detected in low amount, CH_3ONO_2 is quite significant and $C_2H_5ONO_2$ is detected. Larger nitrites or nitrates are not detected, either due to their low mixing ratio or due to fragmentation of the protonated species. Interestingly, peroxyacetyl nitrate (PAN) corresponding to $C_2H_4NO_5^+$ ion, was detected at *m*/*z* 122 in a similar amount as methyl nitrate. The formation of PAN can be explained by NO_2 association with $CH_3C(=O)O$–O radical, resulting from O_2 association with $CH_3C{=}O$. The latter radical might be formed by H abstraction

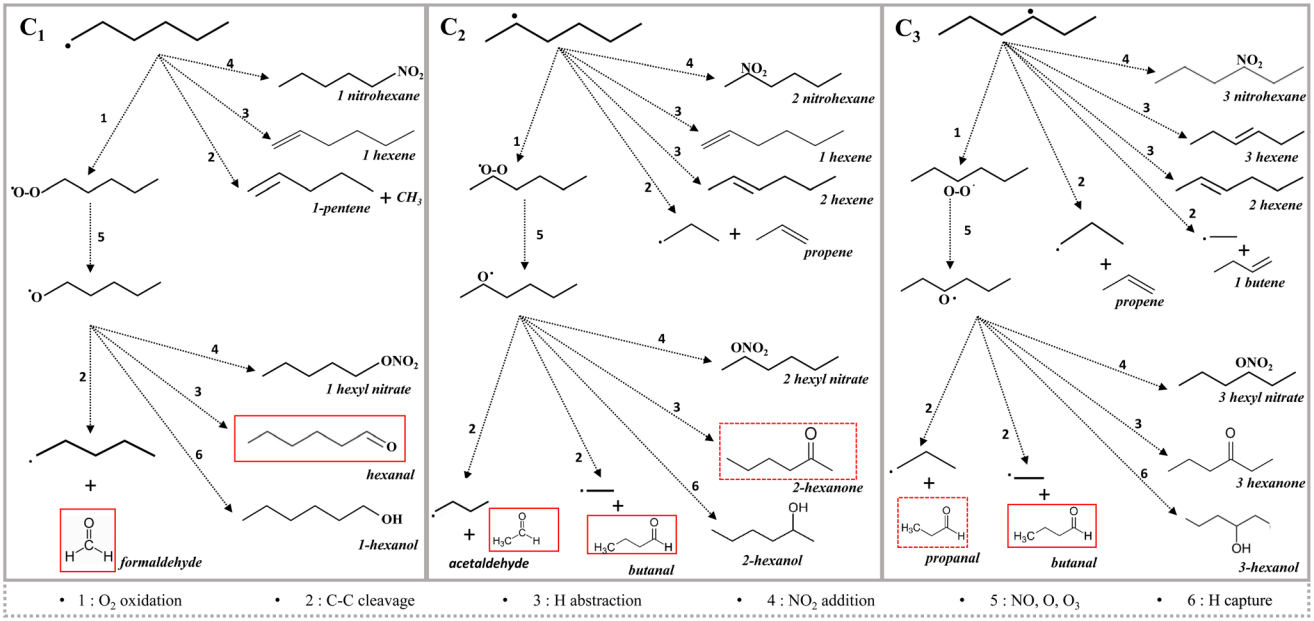

Fig. 10 Proposed mechanism for by-product formation that shows the three main reaction channels for the initiation reactions.

from acetaldehyde, in analogy with the atmospheric process of PAN formation.

In the same manner, the formation of alcohols by H from hexoxy or smaller radicals by H abstraction on another species is not observed except for methanol, but protonation of many alcohols by H_3O^+ is known to be accompanied by dehydration and/or fragmentation. In this case, the resulting ions are identical to those issued from *n*-hexane reaction with H_3O^+.

This mechanism does not include the reactivity of nitrogen metastable states, as observed for other molecules,[50] that lead to the formation of HCN and H_2 in very small amounts.

4 Conclusions

In this study, we present the results obtained for the degradation of *n*-hexane at low mixing ratios in a DBD reactor.

To follow the evolution of the multitude of molecules at the exit of the plasma, different analytical methods were used. For the chemical ionization measurements, two precursor ions were used: O_2^+ to follow mainly *n*-hexane and H_3O^+ to follow organic by-products.

The rate coefficients of the ion precursors with *n*-hexane were remeasured in our experimental conditions for a better quantification. The association of the two precursors has allowed to quantify both *n*-hexane (O_2^+) and most of its degradation by-products (H_3O^+) in real-time and simultaneously on the same sample. O_2^+ precursor also allows the detection of additional degradation products such as nitrogen oxides or ethylene. Moreover, comparing the O_2^+ and H_3O^+ results supports the consistency of product identification.

A satisfying agreement between Micro GC and mass spectrometry measurements of *n*-hexane mixing ratios was observed, confirming that the efficiency of the degradation is higher for low mixing ratios injected.

Only a small proportion of carbon from treated *n*-hexane appears as CO_2 after degradation. The remaining consists of carbon monoxide, carbon-containing by-products, and solid carbonaceous particles (soots), which may be deposited in the reactor or driven by the gas flow. Aldehydes are the main by-products detected with small oxygenated compounds, alkenes, nitrite, and nitrate compounds.

Understanding the mechanisms of degradation becomes necessary with the presence of hazardous compounds in the treated effluent, and a simplified mechanism of by-product formation is proposed. The nature and distribution of the main by-products suggest the hypothesis that oxidation beginning with O_2 addition on a hydrocarbon radical is its most probable reaction in air atmosphere.

The presence of hazardous compounds such as ozone and nitrogen oxide by-products formed are undesirable in the context of industrial applications for depollution. This can be remedied by the addition of a complementary oxidation technique to the plasma, such as catalysis, which is proven to have high removal efficiency and low by-product formation.

Author contributions

Perla Trad: Conceptualization, data curation, formal analysis, investigation, methodology, validation, visualization, writing – original draft, writing – review & editing; Nicole Blin-Simiand: Conceptualization, funding acquisition, supervision, writing – original draft, writing – review & editing; Pascal Jeanney: Conceptualization, resources, software; Stéphane Pasquiers: Writing – original draft, writing – review & Editing; Joel

Lemaire: Writing – review & editing; Essylt Louarn: Writing – review & editing; Hélène Mestdagh: Writing – review & editing; Michel Heninger: Conceptualization, data curation, formal analysis, writing – original draft, writing – review & editing.

Conflicts of interest

There are no conflicts to declare.

Acknowledgements

This work was supported by the Institut National de Recherche et de Sécurité (INRS) [Grant Number 170429], and by Région Ile-de-France (research project n°16016327 Diagplas - Sésame 2016).

References

1 N. Bertrand and F. Clerc, *Hyg. Secur. Trav.*, 2011, **4**, 31–44.
2 A. Emili and G. Mater, *Hyg. Secur. Trav.*, 2018, **1**, 72–74.
3 S. Pasquiers, M. Heninger, N. Blin-Simiand, J. Lemaire, G. Bauville, B. Bournonville, E. Louarn, F. Jorand and H. Mestdagh, *J. Phys. D: Appl. Phys.*, 2018, **51**, 425201.
4 S. Li, X. Dang, X. Yu, G. Abbas, Q. Zhang and L. Cao, *Chem. Eng. J.*, 2020, **388**, 124275.
5 R. Cimerman, D. Racková and K. Hensel, *J. Phys. D: Appl. Phys.*, 2018, **51**, 274003.
6 T. Zhu, J. Li, Y.-q. Jin, Y. Liang and G. Ma, *Int. J. Environ. Sci. Technol.*, 2008, **5**, 375–384.
7 C. Klett, X. Duten, S. Tieng, S. Touchard, P. Jestin, K. Hassouni and A. Vega-González, *J. Hazard. Mater.*, 2014, **279**, 356–364.
8 S. Thomas, N. Blin-Simiand, M. Héninger, P. Jeanney, J. Lemaire, L. Magne, H. Mestdagh, S. Pasquiers and E. Louarn, *J. Am. Soc. Mass Spectrom.*, 2020, **31**, 1579–1586.
9 T. Sato, M. Kambe and H. Nishiyama, *JSME Int. J., Ser. B*, 2005, **48**, 432–439.
10 K. L. L. Vercammen, A. A. Berezin, F. Lox and J.-S. Chang, *J. Adv. Oxid. Technol.*, 1997, **2**, 312–329.
11 L. A. Rosocha and R. A. Korzekwa, *J. Adv. Oxid. Technol.*, 1999, **4**, 247–264.
12 R. Hackam and H. Aklyama, *IEEE Trans. Dielectr. Electr. Insul.*, 2000, **7**, 654–683.
13 H.-H. Kim, *Plasma Processes Polym.*, 2004, **1**, 91–110.
14 J. Van Durme, J. Dewulf, C. Leys and H. Van Langenhove, *Appl. Catal., B*, 2008, **78**, 324–333.
15 H. L. Chen, H. M. Lee, S. H. Chen, M. B. Chang, S. J. Yu and S. N. Li, *Environ. Sci. Technol.*, 2009, **43**, 2216–2227.
16 A. M. Vandenbroucke, R. Morent, N. De Geyter and C. Leys, *J. Hazard. Mater.*, 2011, **195**, 30–54.
17 G. Xiao, W. Xu, R. Wu, M. Ni, C. Du, X. Gao, Z. Luo and K. Cen, *Plasma Chem. Plasma Process.*, 2014, **34**, 1033–1065.
18 F. Thévenet, L. Sivachandiran, O. Guaitella, C. Barakat and A. Rousseau, *J. Phys. D: Appl. Phys.*, 2014, **47**, 224011.
19 X. Feng, H. Liu, C. He, Z. Shen and T. Wang, *Catal. Sci. Technol.*, 2018, **8**, 936–954.
20 R. Mével, K. Chatelain, P. Boettcher, G. Dayma and J. Shepherd, *Fuel*, 2014, **126**, 282–293.
21 Z. Wang, O. Herbinet, Z. Cheng, B. Husson, R. Fournet, F. Qi and F. Battin-Leclerc, *J. Phys. Chem. A*, 2014, **118**, 5573–5594.
22 K. Zhang, C. Banyon, C. Togbé, P. Dagaut, J. Bugler and H. J. Curran, *Combust. Flame*, 2015, **162**, 4194–4207.
23 S. Kudryashov, G. Shchegoleva, E. Sirotkina and A. Y. Ryabov, *High Energy Chem.*, 2000, **34**, 112–115.
24 E. Marotta, A. Callea, X. Ren, M. Rea, C. Paradisi, *et al.*, *Int. J. Plasma Environ.*, 2007, **1**, 39–45.
25 E. Marotta, A. Callea, M. Rea and C. Paradisi, *Environ. Sci. Technol.*, 2007, **41**, 5862–5868.
26 E. Marotta, A. Callea, X. Ren, M. Rea and C. Paradisi, *Plasma Processes Polym.*, 2008, **5**, 146–154.
27 Q. Jin, B. Jiang, J. Han and S. Yao, *Chem. Eng. J.*, 2016, **286**, 300–310.
28 D. Smith, P. Španěl, N. Demarais, V. S. Langford and M. J. McEwan, *Mass Spectrom. Rev.*, 2023, e21835.
29 F. Piel, M. Müller, K. Winkler, J. Skytte af Sätra and A. Wisthaler, *Atmos. Meas. Tech.*, 2021, **14**, 1355–1363.
30 J. Lemaire, S. Thomas, A. Lopes, E. Louarn, H. Mestdagh, H. Latappy, J. Leprovost and M. Heninger, *Sensors*, 2018, **18**, 1415.
31 W. Lindinger, A. Hansel and A. Jordan, *Int. J. Mass Spectrom. Ion Processes*, 1998, **173**, 191–241.
32 B. Yuan, A. R. Koss, C. Warneke, M. Coggon, K. Sekimoto and J. A. de Gouw, *Chem. Rev.*, 2017, **117**, 13187–13229.
33 S. Thomas, N. Blin-Simiand, M. Héninger, P. Jeanney, J. Lemaire, L. Magne, H. Mestdagh, S. Pasquiers and E. Louarn, *Phys. Chem. Chem. Phys.*, 2022, **24**, 20553–20564.
34 A. S. Chiper, N. Blin-Simiand, M. Heninger, H. Mestdagh, P. Boissel, F. Jorand, J. Lemaire, J. Leprovost, S. Pasquiers, G. Popa, *et al.*, *J. Phys. Chem. A*, 2010, **114**, 397–407.
35 T. Guo, G. Cheng, G. Tan, L. Xu, Z. Huang, P. Cheng and Z. Zhou, *Chemosphere*, 2021, **264**, 128430.
36 M. Heninger, H. Mestdagh, E. Louarn, G. Mauclaire, P. Boissel, J. Leprovost, E. Bauchard, S. Thomas and J. Lemaire, *Anal. Chem.*, 2018, **90**, 7517–7525.
37 A. M. Ellis and C. A. Mayhew, in *Chemical Ionization: Chemistry, Thermodynamics and Kinetics*, John Wiley & Sons, Ltd, 2014, ch. 2, pp. 25–48.
38 C. Dehon, J. Lemaire, M. Heninger, A. Chaput and H. Mestdagh, *Int. J. Mass Spectrom.*, 2011, **299**, 113–119.
39 H. Latappy, J. Lemaire, M. Heninger, E. Louarn, E. Bauchard and H. Mestdagh, *Int. J. Mass Spectrom.*, 2016, **405**, 13–23.
40 C. Le Vot, J. Lemaire, P. Pernot, M. Heninger, H. Mestdagh and E. Louarn, *J. Mass Spectrom.*, 2018, **53**, 336–352.
41 T. Wróblewski, L. Ziemczonek, K. Szerement and G. P. Karwasz, *Czech J. Phys.*, 2006, **56**, B1110–B1115.
42 T. Su and W. J. Chesnavich, *J. Chem. Phys.*, 1982, **76**, 5183–5185.

43 W. E. Wallace, *NIST chemistry webbook, NIST standard reference database*, 2018, p. 20899.
44 G. J. Francis, P. F. Wilson, D. B. Milligan, V. S. Langford and M. J. McEwan, *Int. J. Mass Spectrom.*, 2007, **268**, 38–46.
45 S. T. Arnold, A. Viggiano and R. A. Morris, *J. Phys. Chem. A*, 1998, **102**, 8881–8887.
46 N. Blin-Simiand, S. Pasquiers and L. Magne, *J. Phys. D: Appl. Phys.*, 2016, **49**, 195202.
47 M. Schiavon, V. Torretta, A. Casazza and M. Ragazzi, *Water, Air, Soil Pollut.*, 2017, **228**, 1–20.
48 S. Pasquiers, W. Faider, N. Blin-Simiand, L. Magne, P. Jeanney and F. Jorand, *Databases*, 2012, **4**, 19–21.
49 Y.-S. Son, J. Kim, I.-Y. Choi and J.-C. Kim, *Environ. Technol.*, 2021, **42**, 2067–2076.
50 S. Pasquiers, N. Blin-Simiand and L. Magne, *Plasma Phys. Controlled Fusion*, 2013, **55**, 124023.